Chinese Chemical Letters 37 (2026) 112409

Contents lists available at ScienceDirect

Chinese Chemical Letters

journal homepage: www.elsevier.com/locate/cclet

Interfacial cascade channels strategy on innovative heterojunction catalysts for superior piezo-photocatalytic wastewater decontamination

Kaiye Gu[a], Junjie Ni[a], Huinan Che[a], Chen Liu[a,*], Yanhui Ao[a,b,*]

[a] Key Laboratory of Integrated Regulation and Resource Development on Shallow Lakes, Ministry of Education, College of Environment, Hohai University, Nanjing 210098, China

[b] Key Laboratory of Jiangxi Province for Persistent Pollutants Prevention Control and Resource Reuse, Nanchang Hangkong University, Nanchang 330063, China

ARTICLE INFO

Article history:
Received 13 August 2025
Revised 17 November 2025
Accepted 12 January 2026
Available online 13 January 2026

Keywords:
Piezo-photocatalysis
Heterojunction
Piezoelectric polarization
Sulfamethoxazole

ABSTRACT

At present, the practical application of photocatalysis is still limited by poor charge carrier separation efficiency. The incorporation of a piezoelectric polarization field is an effective strategy to enhance the photogenerated charge transport rate and strengthen the photocatalytic activity. In this work, a $NaNbO_3$/AgI (NBO/AgI) heterojunction was fabricated for the efficient piezo-photocatalytic degradation of sulfamethoxazole (SMZ). 91.6 % of SMZ was degraded within 30 min, which far surpasses degradation under individual photocatalysis or piezocatalysis. Density functional theory (DFT) calculations reveal that electron cloud interactions form interfacial cascade channels at the NBO/AgI heterojunction interface, facilitating charge transport. Meanwhile, the piezoelectric polarization field promotes the separation and migration of photogenerated charges, inducing high-efficiency piezo-photocatalytic performance. The piezo-photocatalytic mechanism was explored by electron paramagnetic resonance, piezo-response force microscopy. Intermediate analysis confirmed the degradation pathways and reduced ecological risks of intermediates. This study provides new insights for the design of piezo-photocatalytic materials, as well as a fresh perspective on the treatment of pollutants in wastewater.

© 2026 Published by Elsevier B.V. on behalf of Chinese Chemical Society and Institute of Materia Medica, Chinese Academy of Medical Sciences.

Recent years have seen a rapid rise in industrialization and healthcare, which has led to an overuse and discharge of antibiotics that has posed a serious threat to environmental security and public health [1]. Among the different types of antibiotics, sulfamethoxazole (SMZ) is a commonly used sulfonamide antibiotic that has been widely used in the treatment of bacterial infections [2]. However, it is important to note that SMZ are difficult to biodegrade and can lead to changes in the bacterial community in the water bodies, which can increase the risk of drug-resistant strains and have negative impacts on aquatic ecosystems and human safety [3,4]. Therefore, there is an imperative need to explore a suitable and cost-effective new technology for antibiotic pollution control in the aquatic environment.

Conventional wastewater treatment methods are often insufficient for SMZ removal, making advanced oxidation processes (AOPs) such as photocatalysis an attractive option [5]. However, the practical application of photocatalysis is hindered by rapid recombination of photogenerated carriers, limited solar utilization, and insufficient active sites [6–8]. To date, numerous methodologies have been adopted for the modification of photocatalysts to enhance their activity and efficiency, including elemental doping [9,10], noble metal deposition [11,12], heterostructure construction [13,14], and co-catalyst modification [15,16]. Among them, there are many investigations that have demonstrated that the application of heterojunctions can effectively improve carrier separation and photocatalytic reaction activity for pollutant degradation [17–20]. Yet, to enhance the photocatalytic performance of heterojunctions in practical applications, it is necessary to further improve the interfacial charge transfer efficiency.

It has been reported that the introduction of a piezoelectric polarization field in the photocatalytic process is conducive to the enhancement of the transport rate of photogenerated carriers and effectively improves the photocatalytic efficiency [21–23]. Sodium niobate ($NaNbO_3$) is a typical perovskite-type oxide that possesses attractive properties like excellent piezoelectric and semiconducting properties at room temperature [24]. Meanwhile, $NaNbO_3$ (NBO) has been widely investigated as an environmentally

* Corresponding authors.
E-mail addresses: liuchen211@hhu.edu.cn (C. Liu), andyao@hhu.edu.cn (Y. Ao).

https://doi.org/10.1016/j.cclet.2026.112409
1001-8417/© 2026 Published by Elsevier B.V. on behalf of Chinese Chemical Society and Institute of Materia Medica, Chinese Academy of Medical Sciences.

friendly photocatalyst based on its non-toxicity and high chemical stability [25]. Unfortunately, the wide band gap of NBO leads to its photocatalytic activity only under ultraviolet (UV) light conditions [26]. In order to make greater utilization of solar energy and to take maximum advantage of the piezoelectric properties of NBO, the development of appropriate piezo-photocatalytic systems is a promising strategy [27]. In contrast, silver iodide (AgI) possesses a moderate band gap, strong visible-light absorption, and ease of synthesis, and is frequently used in heterojunction design [28,29]. Thus, combining NBO with AgI is therefore expected to integrate the visible-light response of AgI with the piezoelectric advantage of NBO, enhancing interfacial charge transfer through the synergistic action of photocatalysis and piezocatalysis.

In this work, NBO/AgI heterojunction catalysts were synthesized through an *in-situ* deposition strategy, with AgI nanoparticles uniformly anchored on NBO substrates. The SMZ degradation performance was systematically evaluated under photocatalysis, piezocatalysis, and combined piezo-photocatalysis. Furthermore, the successful construction of heterojunctions was systematically verified by various characterizations, and the potential mechanism of piezoelectric photocatalysis was elucidated by DFT calculations, which revealed the essential role of the internal polarized electric field induced by the piezoelectric effect in the carrier transfer process. Analysis of degradation intermediates confirmed the effective degradation of SMZ by the NBO/AgI piezo-photocatalytic system, underscoring its potential as a green and sustainable treatment technology.

NBO/AgI heterojunction samples were constructed by *in-situ* growth of AgI on NBO substrate by the deposition-precipitation method (Text and Fig. S1 in Supporting information) [30]. The crystalline structure and vibrational characteristics of the samples were analyzed by XRD and Raman spectroscopy. As shown in Fig. S2 (Supporting information), the XRD pattern of pure NBO nanorods matches well with the orthorhombic phase of $NaNbO_3$, while the characteristic peaks of AgI correspond to hexagonal β-AgI [27,31]. In the NBO/AgI-3 composite, diffraction peaks from both phases are clearly present, confirming the coexistence of NBO and AgI. Raman spectra further confirm that NBO possesses an octahedral structure, which remains well preserved after AgI incorporation. To understand the chemical composition and binding states of catalysts, NBO, AgI, and NBO/AgI-3 were analyzed by X-ray photoelectron spectroscopy (XPS). For pristine AgI (Fig. 1a), Ag $3d_{5/2}$ and Ag $3d_{3/2}$ peaks at 368.5 and 374.5 eV confirmed the +1 oxidation state of Ag [32]. In NBO/AgI-3, these peaks shifted by

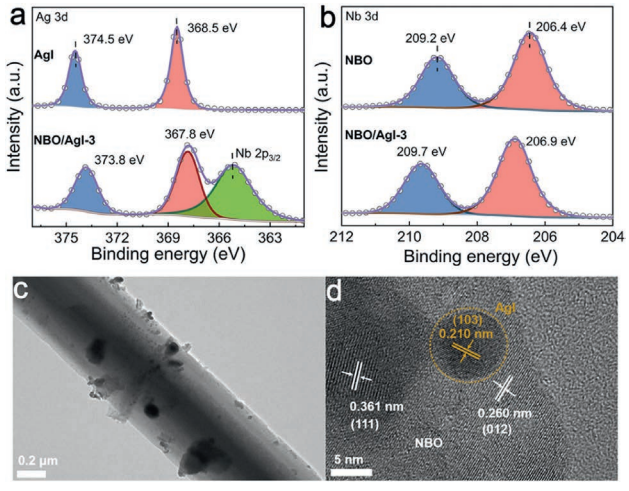


Fig. 1. High-resolution XPS spectra of samples in the regions of (a) Ag 3d and (b) Nb 3d. (c) TEM and (d) HRTEM images of NBO/AgI-3.

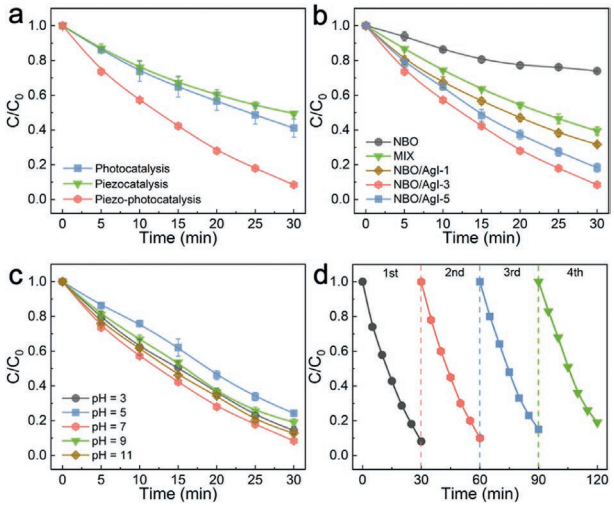


Fig. 2. (a) Comparison of the piezocatalytic, photocatalytic, and piezo-photocatalytic degradation of SMZ in the presence of NBO/AgI-3. (b) Piezo-photocatalysis degradation efficiency for as-prepared samples. (c) SMZ degradation curve under NBO/AgI-3 of different pH. (d) Cyclic stability of NBO/AgI-3 under piezo-photocatalytic.

−0.7 eV to 367.8 and 373.8 eV, respectively. In addition, the peak at 365.3 eV was attributed to Nb $2p_{3/2}$. Fig. 1b shows that Nb in NBO exhibits two characteristic peaks at 206.4 and 209.2 eV, which shift by about 0.5 eV towards higher binding energy in NBO/AgI-3 after AgI coupling. According to the above research and Fig. S3 (Supporting information), Ag 3d and I 3d peaks shifted negatively, whereas Na 1s, Nb 3d, and O 1s peaks shifted positively, evidencing interfacial electronic interaction and electron transfer from NBO to AgI. Transmission electron microscopy (TEM) and high-resolution transmission electron microscopy (HRTEM) were employed to characterize the morphology and micromorphology of materials. As shown in Figs. S4a and b (Supporting information), the NBO exhibits a rod-like structure. The 0.361 nm distance measured by HRTEM corresponds to the NBO (111) plane. Fig. 1c reveals that AgI nanoparticles grow on the surface of NBO nanorods, forming a well-defined and intimate contact interface. Furthermore, HRTEM of the composite sample (Fig. 1d) clearly exhibits an interface between NBO and AgI, in which 0.361, 0.260, and 0.210 nm interplanar distances are assigned to the (111) and (012) planes of NBO and the (103) crystal plane of AgI. Elemental mapping (Figs. S4c and d in Supporting information) revealed uniform distribution of Na, Nb, and O in NBO nanorods, while the even dispersion of Na, Nb, O, I, and Ag in NBO/AgI-3 confirms the homogeneous growth of AgI nanoparticles on NBO surfaces. These results verify the successful introduction of AgI into NBO and the formation of the NBO/AgI-3 heterojunction.

To evaluate the catalytic performance of the heterojunction, the degradation rate of sulfamethoxazole (SMZ) was compared under different conditions. It can be seen from Figs. 2a and b and Fig. S5 (Supporting information) that among the several heterojunction ratios synthesized, the NBO/AgI-3 shows optimal piezo-photocatalytic degradation performance, achieving 91.6% degradation of SMZ in 30 min. Fig. S6 (Supporting information) illustrates that the specific surface area is not a dominant factor in the degradation experiments, as confirmed by the reduced specific surface area of the NBO/AgI-3 composites compared to NBO. Specifically, with simultaneous visible light and ultrasonic vibration, piezo-photocatalysis had a significantly higher degradation effect than the individual photocatalysis and piezocatalysis processes. These results clearly indicate that the constructed NBO/AgI heterojunction effectively promotes the synergistic coupling be-

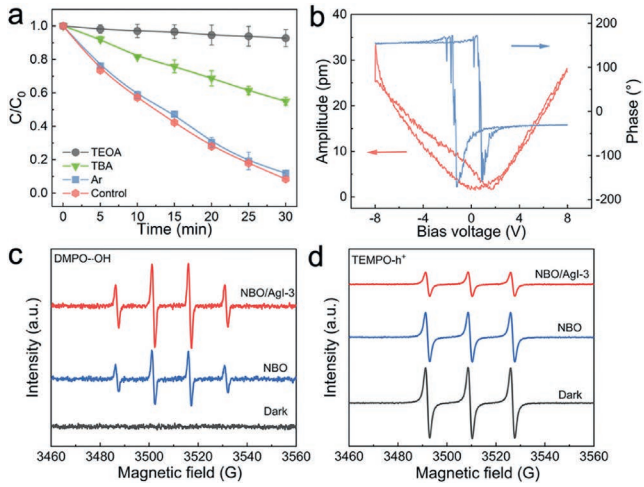


Fig. 3. (a) SMZ degradation in piezo-photocatalytic process using different scavengers. (b) The amplitude-voltage curves and phase hysteresis loop from PFM of NBO/AgI-3. The ESR signals for (c) DMPO-·OH and (d) TEMPO-h^+.

tween photocatalysis and piezocatalysis. In addition, in order to assess the adaptability of the system to the practical environment, the piezo-photocatalytic activity of NBO/AgI-3 for SMZ degradation under different cut-off wavelengths (Fig. S7 in Supporting information) and disparate pH was examined (Fig. 2c). The NBO/AgI-3 composite exhibited efficient piezo-photocatalytic activity across a wide spectral range and maintained over 75 % degradation efficiency under both acidic (pH 5) and alkaline (pH 11) conditions, demonstrating its suitability for practical applications in diverse aqueous environments. According to Fig. 2d, the degradation percent of SMZ for the NBO/AgI-3 still reached 81.0 % after 4 cycles, suggesting its high piezo-photocatalysis stability. Furthermore, after 4 cycles, the XRD pattern of NBO/AgI-3 remained identical to that before reaction, confirming its excellent structural stability and recyclability (Figs. S8 and S9 in Supporting information).

With the aim of analyzing the degradation mechanisms more clearly, the capture experiment was used to investigate the primary active species in the process of piezo-photocatalytic degradation of SMZ. As delineated in Fig. 3a and Fig. S10 (Supporting information), the degradation efficiency of SMZ decreased to 7.2 % and 45.0 % within 30 min upon addition of TEOA (h^+ scavenger) and TBA (·OH scavenger), respectively, confirming that h^+ and ·OH serve as the dominant reactive species. Notably, the introduction of Ar (to eliminate dissolved oxygen) shows a negligible effect on SMZ degradation, indicating minimal involvement of $\cdot O_2^-$ in the process. Moreover, Fig. 3b presents characteristic butterfly-shaped amplitude loops accompanied by well-defined phase hysteresis curves under an applied bias of ±8 V. Fig. S11 (Supporting information) shows that the amplitude and phase images of the NBO/AgI-3 heterojunction samples at a bias field from −8 V to +8 V clearly evidence the polarization reversal behavior of the NBO/AgI-3 heterojunction. These piezoresponse force microscopy (PFM) measurements reveal pronounced phase inversion in the NBO/AgI-3 composites, providing definitive evidence of its exceptional piezoelectric response. Reactive species were further investigated through ESR measurements. Figs. 3c and d and Fig. S12 (Supporting information) display the characteristic signals of TEMPO-h^+ and DMPO-·OH detected in both NBO/AgI-3 and NBO samples under light-ultrasonic conditions. These collective results demonstrate that h^+ and ·OH are the principal active species responsible for SMZ degradation in the piezo-photocatalytic system. Relevant piezoelectric simulations, bandgap analysis, and electrochemical characterizations are provided in Figs. S13-S15 (Supporting information).

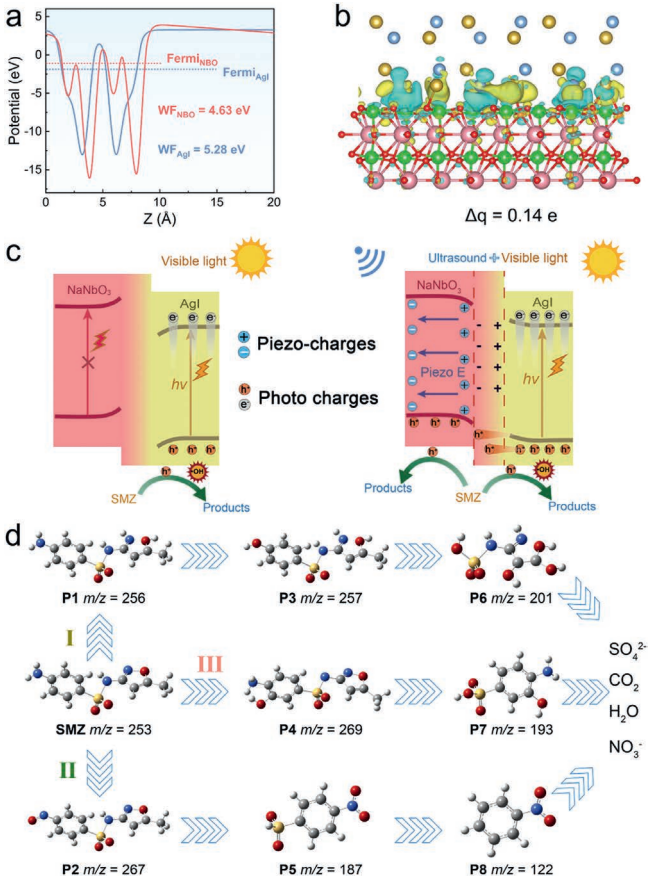


Fig. 4. (a) The work function of NBO and AgI. (b) Charge density difference for the NBO/AgI. (c) Schematic diagrams of the NBO/AgI heterojunction under light and simultaneous light and ultrasound. (d) Proposed degradation pathways of SMZ.

In order to have an insight into the interfacial interactions and charge transfer mechanisms of NBO/AgI-3 heterojunction, density functional theory (DFT) calculations were performed. As shown in Fig. 4a, the work function for NBO and AgI was determined to be 4.63 eV and 5.28 eV, respectively, by aligning the Fermi level to the vacuum level. Since the work function of AgI is higher than that of NBO, the electrons are transferred from NBO to AgI in the heterojunction structure, which is consistent with the XPS analysis. Furthermore, the charge density difference analysis Fig. 4b and Fig. S16 (Supporting information) provide further confirmation of interfacial interactions and electron transfer in the NBO/AgI heterojunction. Quantitative analysis reveals distinct regions of charge depletion in NBO and corresponding charge accumulation in AgI, with a calculated net electron transfer of 0.14 e. Specifically, significant electron density accumulation is observed around I atoms in AgI, while pronounced depletion occurs at Nb atoms in NBO, demonstrating strong interatomic interactions at the heterojunction interface. Therefore, according to DFT calculations, there is a distinct redistribution of electrons at the NBO/AgI interface. The electron cloud interaction of interfacial atoms forms an interfacial cascade channel that facilitates efficient electron migration between NBO and AgI [33].

Based on the analyses above, a plausible degradation mechanism is proposed for the NBO/AgI system under piezo-photocatalytic conditions (Fig. 4c). Due to its wide band gap, NBO cannot be excited by visible light, and thus under illumination, photogenerated carriers are generated only in AgI. Electrons migrate to the CB while holes remain in the VB, where they oxidize pollutants directly or *via* ·OH formation. Nevertheless, the lack of

a strong driving force results in significant carrier recombination. Upon ultrasonication, the piezoelectric effect in NBO generates interfacial polarization charges, inducing band bending in both components and forming an electric field across the heterojunction [34,35]. Under simultaneous light and ultrasonic excitation, this field promotes hole transfer from the VB of AgI to that of NBO and facilitates their migration to the catalyst surface, thereby enhancing interfacial charge separation and carrier transport. As a result, more holes and •OH are available for oxidative degradation, leading to markedly improved piezo-photocatalytic performance.

Further investigation of the degradation process of SMZ by the NBO/AgI piezo-photocatalytic system was conducted through theoretical calculations. Relevant pollutant calculations are presented in Fig. S17 and Table S1 (Supporting Information). The primary intermediate products formed during the degradation of SMZ were detected by HPLC-MS (Fig. S18 and Table S2 in Supporting information). Three possible degradation pathways for SMZ were proposed and depicted in Fig. 4d. In pathway I, the isoxazole ring of SMZ undergoes nucleophilic attack, leading to ring-opening and the formation of intermediate **P1** (*m/z* 256). Subsequent oxidation of the amino group of **P1** results in the generation **P3** (*m/z* 257). Finally, oxidation of the benzene ring in **P3** produces **P6** (*m/z* 201). In pathway II, electrophilic substances attack the N7 atom of SMZ, forming the oxidation by-product **P2** (*m/z* 267). The S14-N17 bond of **P2** is then cleaved through oxidation, yielding **P5** (*m/z* 187), which undergoes desulfurization to eventually form the by-product **P8** (*m/z* 122). In pathway III, hydroxyl radicals initially attack the C2 and C6 position of SMZ, generating hydroxylated SMZ (**P4**, *m/z* 269). Reactive species then cleave the S14-N17 bond of **P4** resulting in the formation of **P7** (*m/z* 193). Ultimately, all intermediates are further degraded by reactive species into smaller molecular fragments or mineralized into CO_2 and H_2O [36,37].

In conclusion, a novel NBO/AgI heterostructure was fabricated *via* a facile deposition–precipitation method. Benefiting from the synergistic effects of visible light and ultrasonic excitation, the NBO/AgI-3 composite exhibited superior piezo-photocatalytic activity, achieving 91.6% sulfamethoxazole degradation within 30 min. Additionally, DFT calculations uncover that the outstanding catalytic activity of NBO/AgI is attributed to the fact that ultrasound can induce a piezoelectric polarization field for efficient bulk charge separation and rapid spatial separation of carriers between interfaces. Analysis of degradation intermediates demonstrated a reduction in the environmental risk of pollutants during the degradation process. This work provides a novel strategy for developing advanced piezo-photocatalytic materials toward efficient water remediation, offering a promising approach to harnessing both mechanical and solar energy for environmental purification.

CRediT authorship contribution statement

Kaiye Gu: Writing – review & editing, Writing – original draft, Visualization, Resources, Methodology, Investigation, Formal analysis, Data curation, Conceptualization. **Junjie Ni:** Methodology, Data curation, Conceptualization. **Huinan Che:** Writing – review & editing, Supervision, Resources, Project administration, Data curation, Conceptualization. **Chen Liu:** Writing – review & editing, Validation, Supervision, Resources, Project administration, Formal analysis, Data curation, Conceptualization. **Yanhui Ao:** Writing – review & editing, Validation, Supervision, Project administration, Funding acquisition, Conceptualization.

Declaration of competing interest

The authors declare that they have no known competing financial interests or personal relationships that could have appeared to influence the work reported in this paper.

Acknowledgments

This work was supported by the Fundamental Research Funds for the Central Universities (No. B250201168), China Postdoctoral Science Foundation (No. 2025M771251), Basic Research Program of Jiangsu (No. BK20251478), Jiangsu Funding Program for Excellent Postdoctoral Talent (No. 2025ZB288), National Key Research and Development Program of China (No. 2022YFC3202402), Key Laboratory of Jiangxi Province for Persistent Pollutants Prevention Control and Resource Reuse (No. 2023SSY02061), Jiangxi Province "Double Thousand Plan", Natural Science Foundation of China (No. 52470184), PAPD.

Supplementary materials

Supplementary material associated with this article can be found, in the online version, at doi:10.1016/j.cclet.2026.112409.

References

[1] W. Xue, X. Shi, J. Guo, et al., Water Res. 253 (2024) 121309.
[2] Y. He, L. Jiang, X. Wu, et al., Water Res. 254 (2024) 121350.
[3] Y. He, L. Liu, Q. Wang, et al., J. Hazard. Mater. 466 (2024) 133558.
[4] Y. Wang, C. Zhou, J. Wu, et al., Chin. Chem. Lett. 31 (2020) 2673–2677.
[5] D. Wang, S. Chen, S. Lai, et al., Chin. Chem. Lett. 35 (2023) 107861.
[6] X. Cheng, Z. Cheng, B. Jing, et al., Water Res. 235 (2023) 119889.
[7] X. Li, Y. Chen, Y. Tao, et al., Chem Catal. 2 (2022) 1315–1345.
[8] W. Jiang, B.Q.L. Low, R. Long, et al., ACS Nano 17 (2023) 4193–4229.
[9] G. Zhang, M. Zhang, X. Ye, et al., Adv. Mater. 26 (2014) 805–809.
[10] J. Huang, D. Li, R. Li, et al., Chem. Eng. J. 374 (2019) 242–253.
[11] J. Fei, J. Li, Adv. Mater. 27 (2015) 314–319.
[12] H. Wu, R. Liang, G. Song, et al., Chin. Chem. Lett. 35 (2024) 109131.
[13] J. Ran, G. Gao, F.T. Li, et al., Nat. Commun. 8 (2017) 13907.
[14] C. Cheng, B. He, J. Fan, et al., Adv. Mater. 33 (2021) 2100317.
[15] H. Zhang, P. Sun, X. Fei, et al., Nat. Commun. 15 (2024) 4453.
[16] L. Qi, Y. Liu, Y. Tang, et al., Appl. Catal. B: Environ. 353 (2024) 124099.
[17] Q. Hou, M. Wang, T. Li, et al., Chem. Eng. J. 464 (2023) 142566.
[18] J. Huang, B. Zhu, D. Song, et al., Chem. Eng. J. 464 (2023) 142784.
[19] C. Du, S. He, Y. Xing, et al., Mater. Today Phys. 27 (2022) 100827.
[20] C. Chu, Y. Qin, C. Ni, et al., Appl. Catal. B: Environ. 341 (2024) 123321.
[21] C. Li, W. Liu, X. Chen, et al., Chin. Chem. Lett. 35 (2024) 109652.
[22] F. Wu, Y. Yu, H. Yang, et al., Adv. Mater. 29 (2017) 1701432.
[23] J. Hu, C. Yu, C. Li, et al., Nano Energy 101 (2022) 107583.
[24] T.Y. Ke, H.A. Chen, H.S. Sheu, et al., J. Phys. Chem. C 112 (2008) 8827–8831.
[25] D. Zhang, J. Qi, H. Ji, et al., Chem. Eng. J. 400 (2020) 125918.
[26] H. Shi, G. Chen, C. Zhang, et al., ACS Catal. 4 (2014) 3637–3643.
[27] S. Singh, N. Khare, Nano Energy 38 (2017) 335–341.
[28] R. Zhou, D. Zhang, P. Wang, et al., Appl. Catal. B: Environ. 285 (2021) 119820.
[29] F. Chen, H. Huang, Y. Zhang, et al., Chin. Chem. Lett. 28 (2017) 2244–2250.
[30] X. Gao, J. Chen, H. Che, et al., Chem. Eng. J. 426 (2021) 131585.
[31] Y.H. Yu, B.B. Huang, H. Wang, et al., J. Colloid Interface Sci. 522 (2018) 82–94.
[32] F. Guo, W. Shi, H. Wang, et al., J. Hazard. Mater. 349 (2018) 111–118.
[33] Y. Wen, W. Liu, P. Wang, et al., Adv. Funct. Mater. 33 (2023) 2308084.
[34] L. Wang, S. Liu, Z. Wang, et al., ACS Nano 10 (2016) 2636–2643.
[35] H. Lv, H. Yin, T. Wang, et al., Mater. Today Phys. 37 (2023) 101212.
[36] H. Li, J. Liu, X. Zhang, et al., Appl. Catal. B: Environ. 376 (2025) 125453.
[37] C. Zhu, M. Yang, B. Jiang, et al., Nat. Commun. 16 (2025) 790.